Scientia Iranica (2024) 31(1), 71–82

Sharif University of Technology
Scientia Iranica
Transactions B: Mechanical Engineering
https://scientiairanica.sharif.edu

Research Note

Energy optimization of water-based hybrid nanomaterials over a wedge-shaped channel

M. Sarfraz* **and M. Khan**

Department of Mathematics, Quaid-i-Azam University, Islamabad 44000, Pakistan.

Received 11 April 2022; received in revised form 29 November 2022; accepted 21 February 2023

KEYWORDS
Heat transfer;
Hybrid fluids;
Jeffery-Hamel flow;
Numerical solutions;
Wedge-shaped channel.

Abstract. Convergent/divergent channels have real-world applications, including the production of fibers, the manipulation of molten metal streams, and the industrial casting of metal. This article intends to discuss the flow and thermal transport of a mixture of nanoparticles, namely, copper and molybdenum oxide, in a base fluid (water) over a wedge-shaped channel. The dissipation effects are taken into account. To understand the thermophysical characteristics of the nanoparticles, the Yamada Ota model is selected. By using similarity transformations, the partial differential equations are converted into ordinary differential equations. The numerical solution is developed by applying the bvp4c built-in MATLAB. The impact of irreversibility effects is also incorporated. Moreover, the outcomes for the wall stress parameter and Nusselt number are calculated as a function of pertinent parameters. It is noted that the momentum and energy of the system are reduced due to accretion in the nanoparticle volume fraction of copper for both hybrid nanofluids and conventional nanofluids. For both convergent and divergent channels, heat transport is an increasing function of Brinkman number. The numerical values of thermal transport are developed for a specific range of Brinkman numbers and decreased for Reynolds numbers. The thermal transport is abridged for hybrid nanofluids more, as compared to mono nanofluids.

1. Introduction

In the fields of science and engineering, as well as in the realm of industrial and architectural works, such as flows through cavities and canals, the study of fluid flow through convergent/divergent walls has incredibly astounding practical implications. The flow of blood via arteries and capillaries in the human body is another illustration of fluid movement along Convergent Channel (CC) or Divergent Channel (DC). They are used in the production of fibers, glasses, papers, and wires when a magnetic field is present. Other practical applications for CC/DC include the preparation of plastic sheets for use in manufacturing, controlling molten metal streams, and manufacturing wires. Over the past years, the widespread applications in plasma generators, chemical vapor deposition reactors, compression or expansion of areas in any machinery, compression of gases, and so forth have obtained additional recognition. The problem of Jeffery-Hamel (J-H) flow and its heat transfer analysis has gained more attention, and it is one of the most practical problems in mechanical, aerospace, and biomechanical

*. *Corresponding author.*
E-mail address: mahnoor@math.qau.edu.pk (M. Sarfraz)

doi: 10.24200/sci.2023.60254.6689

engineering. In this model, the flow is generated by a CC/DC through a source/sink. Jeffery [1] and Hamel et al. [2] pioneered this model, and after that, numerous research studies have been conducted because of its novelty in applications, and it constitutes one of the exact solutions to Navier-Stokes equations. Axford [3] scrutinized the J-H problem with the influence of the magnetic field exterior on the conducting fluid. He reported that the Reynolds number and magnetic field behaved as controlling parameters for the flow and angle of inclination of the walls. Hamadiche et al. [4], in their work, examined the temporal stability of this problem in a DC. In the existence of a homogeneous magnetic field, the flow analysis of viscous fluid in a CC/DC was studied by Makinde and Mhone [5]. They applied the technique of perturbation series summation and refinement to determine the solutions. Numerous studies have been conducted to compute the analytical and numerical solution of this problem since they are easier to calculate. Esmaeilpour and Ganji [6] used the optimal homotopy perturbation method and the Runge-Kutta method for the analytical and numerical solutions, respectively. Mahmood et al. [7] also considered SHPM to compute the solution of the flow and energy equations. The exact solutions of J-H flow were calculated in Refs. [8–10]. The effects of this shock on the boundary layer parameter were studied by Amiri et al. [11] in their research. Analytically, adiabatic, inviscid, and one-dimensional models of the water vapor flow with the potential for nucleation were studied. Heydari [12] conducted a numerical analysis of hydrodynamics and heat transport of airflow in a constrained microchannel. He considered the effects of geometry, stagnation pressure, temperature, and applied heat flux at the walls. The influence of a uniform magnetic field on a nanofluid flow that is filling a porous material inside parallel sheets is computed by Ahmad et al. [13].

Because of its numerous applications, such as accelerators, cooling systems, flow meters, MHD generators, magnetic endoscopy, cancer tumor therapy, and so on, the study of heat transport has gotten great interest in the field of engineering and biosciences. The phenomenon of heat transport analyzes the production, conversion, and exchange of energy by different methods, for instance, diffusion, convection, and radiation. The phenomenon purely depends on the size and shape of the nanoparticles under consideration. Two or more distinct nanoparticles can be added to the base fluids to create hybrid nanofluids. They are added to the base fluid to improve thermal conductivity. They often produce greater k values than those seen in pure fluids or in nanofluids made up of only one particle. Biosensors, doppler and sympathetic cooling, fire alarm, thermostat, and magnetic preservation are some of their practical applications. The study to enhance the heat transport characteristics of fluid was pioneered by Choi and Eastman [14]. He used the term nanofluid, which refers to nano-sized particles suspended in a base fluid. Sheikholeslami et al. [15] conducted an analytical investigation of J-H nanofluid flow by using the reconstruction of variation of the iteration method. The effects of solar radiation on the flow and thermal transport of non-parallel plates were examined by Kumar et al. [16]. The heat transfer analysis of hybrid nanofluid flow with Ohmic heating and heat source-sink was scrutinized by Sarfraz et al. [17]. Research related to energy transport analysis of the non-parallel plates with convergent and divergent flow and hybrid nanofluid flow are inspected in Refs. [18,19]. Berrehal and Makinde [20] calculated the approximate solutions of water-based nanofluid J-H flow by using the Runge-Kutta-Fehlberg (RKF) method. The CC/DC with entropy generation and magnetohydrodynamic for copper-water nanofluid flow were studied by Das and Nasa [21]. They noticed a significant increment in the entropy generation of the system.

Motivated by the foregoing articles, this study intends to discuss the flow and thermal transport of water-based nanofluid on a wedged-shaped channel. Here, water is used as a base fluid with copper and molybdenum oxide particles immersed in it. The possible applications include the production of fibers, glasses, papers, and wires when a magnetic field is present. Other practical applications for convergent/divergent channels include the preparation of plastic sheets for use in manufacturing, controlling molten metal streams, and manufacturing wires. Hybrid nanofluids have extraordinary electromechanical properties, and their micro size enables them to be a part of different practical applications in various fields. Their high thermal and electrical properties and large surface area have proven to be successful adsorbing agents in the diagnosis of diseases and substances (in pharmacy and medicine). The present study can be beneficial in these fields. They have been discovered to be a promising antioxidant and are valuable for the process of tissue generation, bio-sensor diagnosis, chiral separation, and pollutant extraction. Molybdenum oxides are adaptable oxide compounds having widely used applications in biosystems, catalysis, chromogenic, electrochromic, electronics, energy storage devices, sensors, field emission devices, lubricants, superconductors, and thermal materials. Copper nanoparticles have two functions: they increase porosity and function as an antibacterial agent, as but less efficiently than other metal nanoparticles (internal surface area and pore volume). The numerical solution is developed by applying bvp4c built-in MATLAB. The values for the wall stress parameter and Nusselt number are calculated as a function of pertinent parameters.

The article is modeled to provide answers to the following important queries:

a. What is the impact of the mixture of nanoparticles on both CC and DC?
b. How is the heat transfer rate modified due to the presence of hybrid nanoparticles, and what is its impact on CC and DC?

2. Problem description

Consider the Jeffery-Hamel hybrid nanofluid flow of an incompressible fluid between two non-parallel inclined plates forming a wedge-shaped channel. The angle of inclination between these plates is 2γ, where the channel is taken as divergent when $\gamma > 0$ and convergent when $\gamma < 0$. The problem is modeled in the cylindrical polar coordinates (r, ϑ, z) to explain the flow and heat transfer analysis in the channel. The dissipation effects are incorporated by taking viscous dissipation. The thermophysical characteristics of the model are also taken into account by using the Yamada Ota model. Moreover, water is used as a base fluid with two distinct nanoparticles, i.e., Cu and MoS_4. It is assumed that the fluid flow is merely radial and depends mainly on r and ϑ; therefore, it has no variation along the z-direction. Moreover, a no-slip condition is used at the boundary. The velocity profile is given as $\mathbf{V} = [\tilde{u}(r,\vartheta), 0, 0]$. Furthermore, it is assumed that there is no variation of fluid temperature $\tilde{T}$ at the centerline when $\vartheta = 0$ The geometrical description of the problem is given in Figure 1. The governing equations for the model are:

$$\tilde{u}_r + \tilde{u} r^{-1} = 0, \tag{1}$$

$$\tilde{u}\tilde{u}_r = -\frac{1}{\varrho_{hn}} p_r + \frac{\mu_{hn}}{\varrho_{hn}} \left(\tilde{u}_{rr} + r^{-1}\tilde{u}_r - r^{-2}\tilde{u} + r^{-2}\tilde{u}_{\vartheta\vartheta} \right), \tag{2}$$

$$0 = -\frac{1}{\varrho_{hn}} p_\vartheta + 2\frac{\mu_{hn}}{\varrho_{hn}} \left(r^{-2}\tilde{u}_{\vartheta\vartheta} \right), \tag{3}$$

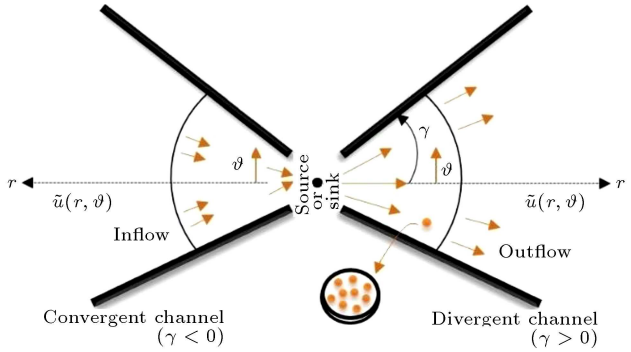

Figure 1. Schematic diagram representing inflow at $\gamma < 0$ and outflow at $\gamma > 0$.

$$\tilde{u}\tilde{T}_r = \frac{k_{hn}}{(\varrho c_p)_{hn}} \left(\tilde{T}_{rr} + r^{-1}\tilde{T}_r + r^{-2}\tilde{T}_{\vartheta\vartheta} \right) + \frac{\mu_{hn}}{(\varrho c_p)_{hn}} \left(2\tilde{u}_r^2 + 2r^{-2}\tilde{u}^2 + r^{-2}\tilde{u}_\vartheta^2 \right) - \frac{16\sigma^* \tilde{T}_w^3}{3k^*(\varrho c_p)_{hn}} \left(\tilde{T}_{rr} + r^{-1}\tilde{T}_r + r^{-2}\tilde{T}_{\vartheta\vartheta} \right). \tag{4}$$

The thermophysical properties are given as (see Sarfraz et al. [17]):

$$\begin{aligned}
\mu_{hn} &= \mu_n (1-\phi_{Cu})^{-2.5} (1-\phi_{MoS_4})^{-2.5}, \\
\varrho_{hn} &= \phi_{MoS_4}\varrho_{MoS_4} + (1-\phi_{MoS_4}) \left[(1-\phi_{Cu})\varrho_n + \phi_{Cu}\varrho_{Cu} \right], \\
(\varrho c_p)_{hn} &= \phi_{MoS_4}(\varrho c_p)_{MoS_4} + (1-\phi_{MoS_4}) \left[(1-\phi_{Cu})(\varrho c_p)_n + \phi_{Cu}(\varrho c_p)_{Cu} \right], \\
\mu_n &= \mu_f (1-\phi_{Cu})^{-2.5}, \\
\varrho_{nf} &= \phi_{Cu}(\varrho_{Cu}) + (1-\phi_{Cu})(\varrho_f), \\
(\varrho c_p)_{nf} &= \phi_{Cu}(\varrho c_p)_{Cu} + (1-\phi_{Cu})(\varrho c_p)_f.
\end{aligned} \tag{5, 6}$$

For the Yamada-Ota model, the thermal conductivity is given by Eqs. (7) and (8) are shown in Box I. The thermophysical properties of engine oil and nanoparticles are presented in Table 1. The conditions at the centerline of the channel are (see Ellahi [8]):

$$\tilde{u}(r,\vartheta) = \tilde{U}_{\max}, \qquad \tilde{u}_\vartheta(r,\vartheta) = 0, \qquad \tilde{T}_\vartheta(r,\vartheta) = 0, \quad \text{at} \quad \vartheta = 0. \tag{9}$$

The conditions at the boundary are:

$$\tilde{u}(r,\vartheta) = 0, \qquad \tilde{T}(r,\vartheta) = \tilde{T}_{wall}, \quad \text{as} \quad \vartheta = \gamma. \tag{10}$$

Since the flow is purely radial, we have:

$$r\tilde{u}(r,\vartheta) \equiv \tilde{f}(\vartheta) \Rightarrow \tilde{u}(r,\vartheta) \equiv r^{-1}\tilde{f}(\vartheta). \tag{11}$$

Introducing the dimensionless velocity, temperature, and degree to reduce Eqs. (2)–(4):

Table 1. Numerical values of the thermophysical properties.

Physical properties		c_p	ϱ	k
Fluid	Water	1910	884	0.1440
Nanoparticles	Copper	425	2600	6600
	MoS_4	796	1600	3000

$$\frac{k_{hn}}{k_n}=\frac{1+\frac{Lk_n}{Rk_{MoS_4}}(\phi_{MoS_4})^{0.2}+\left(1-\frac{k_n}{k_{MoS_4}}\right)\phi_{MoS_4}\left(\frac{L}{R}\right)(\phi_{MoS_4})^{0.2}+2\phi_{MoS_4}\left(\frac{k_{MoS_4}}{k_{MoS_4}-k_n}\right)\ln\left(\frac{k_{MoS_4}+k_n}{2k_n}\right)}{(1-\phi_{MoS_4})+2\phi_{MoS_4}\left(\frac{k_n}{k_{MoS_4}-k_n}\right)\ln\left(\frac{k_{MoS_4}+k_n}{2k_n}\right)}, \quad (7)$$

$$\frac{k_n}{k_f}=\frac{1+\frac{Lk_n}{Rk_{Cu}}(\phi_{Cu})^{0.2}+\left(1-\frac{k_n}{k_{Cu}}\right)\phi_{Cu}\left(\frac{L}{R}\right)(\phi_{Cu})^{0.2}+2\phi_{Cu}\left(\frac{k_{Cu}}{k_{Cu}-k_n}\right)\ln\left(\frac{k_{Cu}+k_n}{2k_n}\right)}{(1-\phi_{Cu})+2\phi_{Cu}\left(\frac{k_f}{k_{Cu}-k_f}\right)\ln\left(\frac{k_{Cu}+k_f}{2k_f}\right)}. \quad (8)$$

Box I

$$\tilde{F}(\zeta)=\frac{\tilde{f}(\vartheta)}{\tilde{f}_{\max}}=\frac{r^{-1}\tilde{f}(\vartheta)}{\tilde{U}_{\max}},\qquad \tilde{H}(\zeta)=\frac{\tilde{T}(r,\vartheta)}{\tilde{T}_w},$$

$$\text{with}\quad \zeta=\frac{\vartheta}{\gamma}, \quad (12)$$

where, for inflow, we have a CC with γ and $\tilde{U}_{\max}<0$, and for outflow, we get a DC with γ and $\tilde{U}_{\max}>0$.

By cross-differentiating Eqs. (2) and (3), we obtain the non-dimensional ordinary differential equations with Boundary Conditions (BCs) as:

$$\tilde{F}'''+2\frac{\mathcal{A}_1}{\mathcal{A}_2}\gamma Re\tilde{F}\tilde{F}'+4\gamma^2\tilde{F}'=0,\qquad \tilde{F}'(0)=0,$$

$$\tilde{F}(0)=1,\qquad \tilde{F}(1)=0, \quad (13)$$

$$\left(1+\frac{R_d}{\mathcal{A}_4}\right)\tilde{H}''+\frac{\mathcal{A}_2}{\mathcal{A}_4}Br\left(4\gamma^2\tilde{F}^2+\tilde{F}'^2\right)=0,$$

$$\tilde{H}'(0)=0,\qquad \tilde{H}(1)=1, \quad (14)$$

where:

$$\mathcal{A}_1=\frac{\varrho_{hn}}{\varrho_n},\qquad \mathcal{A}_2=\frac{\mu_{hn}}{\mu_n},$$

$$\mathcal{A}_3=\frac{(\varrho c_p)_{CNT}}{(\varrho c_p)_n},\qquad \mathcal{A}_4=\frac{k_{hn}}{k_n}.$$

The dimensionless parameters include the Reynolds number $Re\left(=\frac{\gamma\tilde{f}_{\max}}{\nu_f}\right)$, the radiation parameter $R_d\left(=\frac{16\sigma^*\tilde{T}_\infty^3}{3k^*k_f}\right)$, the Brinkman number $Br(=PrEc)$ the Prandtl number $Pr\left(=\frac{\tilde{f}_{\max}(\varrho c_p)_f}{k_f}\right)$, and the Eckert number $Ec\left(=\frac{(\tilde{U}_{\max})^2}{c_p\tilde{T}_w}\right)$.

2.1. Physical quantities of engineering interest

The coefficient of skin friction $C_{\tilde{f}}$ with wall stress τ_{wall} is defined as:

$$C_{\tilde{f}}=\frac{\tau_{wall}}{\varrho_n\tilde{U}_{\max}^2}=\frac{1}{Re(1-\phi_{Cu})^{2.5}(1-\phi_{MoS_4})^{2.5}}\tilde{F}'(1),$$

$$\text{with}\qquad \tau_{wall}=\mu_{hn}\left(\frac{1}{r}\frac{\partial\tilde{u}}{\partial\vartheta}\right)_{\vartheta=\gamma}, \quad (15)$$

and the Nusselt number Nu with heat flux ψ_q is:

$$Nu=\frac{r\psi_q}{k_n\left(\tilde{T}_w\right)}=-\left(\frac{k_{hn}}{k_n}+R_d\right)\gamma^{-1}\tilde{H}'(1),$$

$$\text{with}\qquad \psi_q=-\left(k_{hn}+\frac{16\sigma^*}{3k^*}\tilde{T}_\infty^3\right)\left(\frac{1}{r}\frac{\partial\tilde{T}}{\partial\vartheta}\right)_{\vartheta=\gamma}. \quad (16)$$

2.2. Thermodynamic irreversibility

Controlling entropy buildup is typically a top priority in contemporary engineering. Identifying the sources of waste/disorders in any system and enhancing the efficiency of any physical equipment is possible via entropy generation evaluation. Reevaluating energy consumption and production habits is necessary due to the limited availability of global energy sources. Thermodynamic transport and viscous dissipation are used to express the rate of local entropy creation of a nanoparticle. The thermodynamic irreversibility effects are incorporated through entropy generation and Bejan number (irreversibility distribution ratio), given as:

$$\tilde{S}_g=\frac{1}{\left(\tilde{T}_w\right)^2}\left[k_{hn}+\frac{16\sigma^*}{3k^*}\tilde{T}_\infty^3\right]\left(r^{-2}\left(\tilde{T}_\vartheta\right)^2\right)+\frac{\mu_{hn}}{\tilde{T}_w}\left(2\tilde{u}_r^2+2r^{-2}\tilde{u}^2+r^{-2}\tilde{u}_\vartheta^2\right), \quad (17)$$

$$\tilde{B}_e=\frac{Entropy\ due\ to\ heat\ transfer}{Total\ entropy}, \quad (18)$$

$$\tilde{N}_g=(\mathcal{A}_4+R_d)\tilde{H}'^2+\frac{\mathcal{A}_1\gamma Br}{Re}\left(\tilde{F}'^2+4\gamma^2\tilde{F}^2\right), \quad (19)$$

$$\tilde{B}_e=\frac{\mathcal{A}_4\tilde{H}'^2}{(\mathcal{A}_4+R_d)\tilde{H}'^2+\frac{\mathcal{A}_1Br\gamma}{Re}\left(\tilde{F}'^2+4\gamma^2\tilde{F}^2\right)}. \quad (20)$$

The Bejan number ranges from $0\le\tilde{B}_e\le1$. When $\tilde{B}_e=0$ fluid friction has a stronger impact than irreversibility effects. Because of heat transfer, irreversibility dominates the flow system at $\tilde{B}_e=1$

However, at $B_e = \frac{1}{2}$ the contributions of fluid friction and heat transfer to entropy production are equal.

2.3. Numerical solution approach

The goal of this section is to provide a numerical solution to our problem. To compute the numerical solution of Eqs. (2)–(4) in MATLAB, we used an in-built function, a finite difference approach, called bvp4c. This method uses the four-stage Lobatto IIIa formula and provides continuous $\mathcal{C}^1$ solutions, controls mesh/error tolerances automatically, and generates a solution to the problem. Shampine et al. [22] further discussed this technique in detail in their book. The first-order ODEs are constructed using the following conversion to use this method:

$$\tilde{F} = Y_1, \quad \tilde{F}^{'} = Y_2, \quad \tilde{F}^{''} = Y_3, \quad \tilde{F}^{'''} = YY_1,$$

$$\tilde{H} = Y_4, \quad \tilde{H}^{'} = Y_5, \quad \tilde{H}^{''} = YY_2, \tag{21}$$

The resulting first-order equations are:

$$YY_1 = -2\frac{\mathcal{A}_1}{\mathcal{A}_2}\gamma ReY_1Y_2 - 4\gamma^2 Y_2,$$

$$Y_1(0) = 1, \quad Y_2(0) = 0, \quad Y_1(1) = 0, \tag{22}$$

$$YY_2 = -\frac{\frac{\mathcal{A}_2}{\mathcal{A}_4}Br\left(4\gamma^2 Y_1^2 + Y_2^2\right)}{\left(1+\frac{R_d}{\mathcal{A}_4}\right)},$$

$$Y_5(0) = 0, \qquad Y_4(1) = 1, \tag{23}$$

$$N_g = (\mathcal{A}_4 + R_d){Y_5}^2 + \frac{\mathcal{A}_1 Br\gamma}{Re}\left({Y_2}^2 + 4\gamma^2{Y_1}^2\right), \tag{24}$$

$$B_e = \frac{\mathcal{A}_4{Y_5}^2}{(\mathcal{A}_4 + R_d){Y_5}^2 + \frac{\mathcal{A}_1 Br\gamma}{Re}\left({Y_2}^2 + 4\gamma^2{Y_1}^2\right)}. \tag{25}$$

2.4. Small-Re asymptotics

Assuming $\tilde{F}(\zeta) = \tilde{F}_0(\zeta) + Re\tilde{F}_1(\zeta) + \cdots$ and $\tilde{H}(\zeta) = \tilde{H}_0(\zeta) + Re\tilde{H}_1(\zeta) + \cdots$. The zeroth and first-order systems of Eqs. (13) and (14) become:

$$\tilde{F}_0^{'''} + 4\gamma^2\tilde{F}_0' = 0, \qquad \tilde{F}_0'(0) = 0,$$

$$\tilde{F}_0(0) = 1, \qquad \tilde{F}_0(1) = 0, \tag{26}$$

$$\tilde{F}_1^{'''} + 2\frac{\mathcal{A}_1}{\mathcal{A}_2}\gamma Re\tilde{F}_0\tilde{F}_0' + 4\gamma^2\tilde{F}_1' = 0,$$

$$\tilde{F}_1'(0) = \tilde{F}_1(0) = \tilde{F}_1(1) = 0, \tag{27}$$

$$\left(1+\frac{R_d}{\mathcal{A}_4}\right)\tilde{H}_0^{''} + \frac{\mathcal{A}_2}{\mathcal{A}_4}Br\left(4\gamma^2\tilde{F}_0^2 + \tilde{F}_0^{'2}\right) = 0,$$

$$\tilde{H}_0^{'}(0) = 0, \qquad \tilde{H}_0(1) = 1, \tag{28}$$

$$\left(1+\frac{R_d}{\mathcal{A}_4}\right)\tilde{H}_1^{''} + \frac{\mathcal{A}_2}{\mathcal{A}_4}Br\left(8\gamma^2\tilde{F}_0\tilde{F}_1 + 2\tilde{F}_0'\tilde{F}_1'\right) = 0,$$

$$\tilde{H}_1'(0) = \tilde{H}_1(1) = 0. \tag{29}$$

For wall stress and coefficient of heat transfer, the equations become $\tilde{F}^{''}(0) \sim \tilde{F}_0^{''}(0) + Re\tilde{F}_1^{''}(0) + \cdots$ and $\tilde{H}^{'}(0) \sim \tilde{H}_0^{'}(0) + Re\tilde{H}_1^{'}(0) + \cdots$, respectively.

3. Discussion of results

The section presents the impact of the pertinent parameters on $\tilde{F}^{'}(\zeta)$ and $\tilde{H}(\zeta)$ with (Cu–MoS_4/H_2O) and (Cu/H_2O) profiles for both CC and DC. The numerical scheme developed to compute the outcomes of the equations is bvp4c in MATLAB. All the parameters are varied one after another, while the value of other parameters is taken constant. The fixed values are $\phi_{Cu} = \phi_{MoS_4} = 0.01, Re\varepsilon\,[1, 20]$, and $Br = 5.0$. In all of the figures, solid lines and dashed lines represent (Cu/H_2O) and (Cu–MoS_4/H_2O) profiles, respectively.

In Figure 2(a)–(d), the impression of nanoparticle volume fraction ϕ_{Cu} on $\tilde{F}^{'}(\zeta)$ and $\tilde{H}(\zeta)$ is noted for the CC and DC. Figure 2(a) and (b) signify the comparison between these two channels for the flow field. It is seen that the velocity profile is diminished due to the increment in ϕ_{Cu}. This is because augmentation in nanoparticle quantity causes a reduction in velocity near the wall. However, the fluid velocity is maximum at the centerline. The impact of inflow and outflow on the hybrid nanofluid particles can be examined through these figures. Molybdenum oxides are adaptable oxide compounds that have widely used applications in biosystems, electronics, energy storage devices, sensors, lubricants, superconductors, and thermal materials. Copper nanoparticles increase porosity and function as an antibacterial agent but are less efficient than other metal nanoparticles (internal surface area and pore volume). It is notable that for $\gamma < 0$, (Cu/H_2O) is dominant over (Cu–MoS_4/H_2O); however, a reverse process is seen for $\gamma > 0$ Figure 2(c) and (d) highlight that heat transport phenomena deteriorate due to enhancing the nanoparticles concentration. This is because of the fact that the fluid flow is reduced, which causes the kinetic energy of the particles to decrease as well. Therefore, the thermal transfer rate lessens as well. It can be perceived that hybrid nanofluid profile (Cu–MoS_4/H_2O) dominates over the mono nanofluid profile (Cu/H_2O).

Figure 3(a)–(c) depict the relationship of the angle of inclination γ on $\tilde{F}^{'}(\zeta)$ and $\tilde{H}(\zeta)$ respectively. Figure 3(a) and (b) give the impact of γ on the velocity profiles. The velocity, thermal, and mass distribution decline as the angle of inclination is enhanced. Physically, with an increment in γ, the fluid motion is diminished near the walls and eventually goes to zero

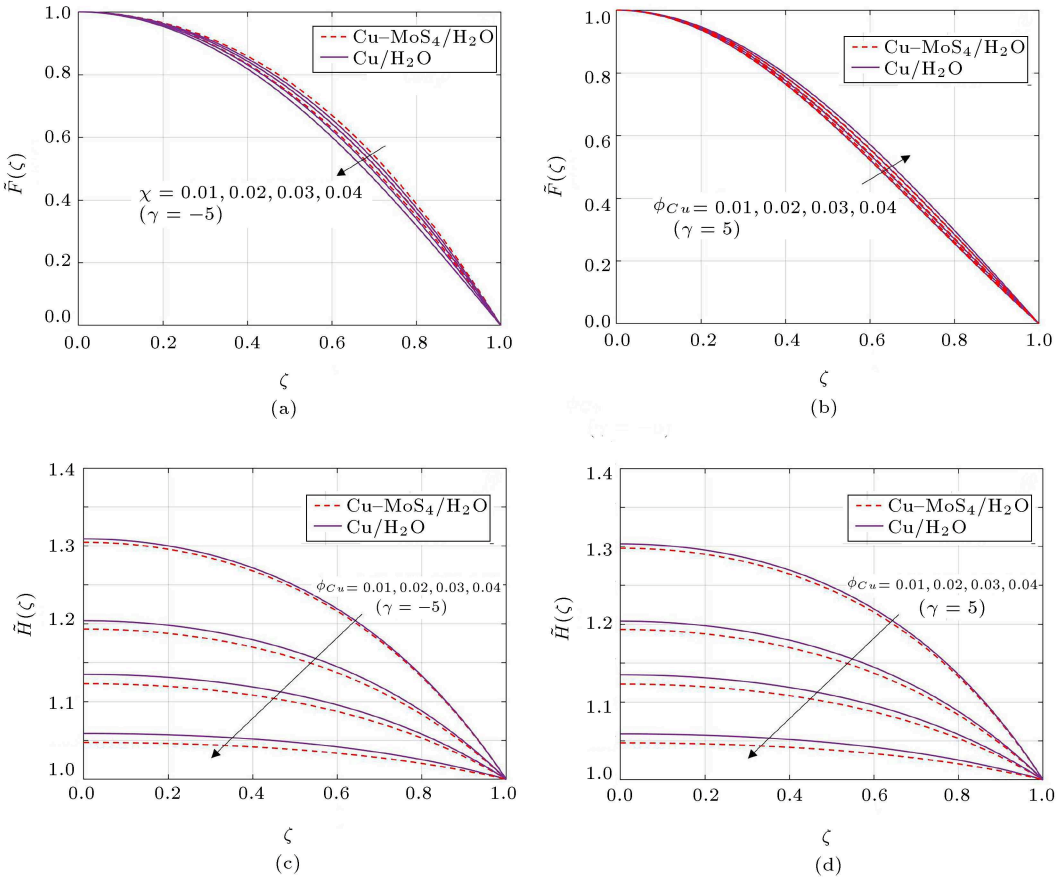

Figure 2. $\tilde{F}'(\zeta)$ and $\tilde{H}(\zeta)$ as a function of ϕ_{Cu} for $\gamma < 0$ and $\gamma > 0$.

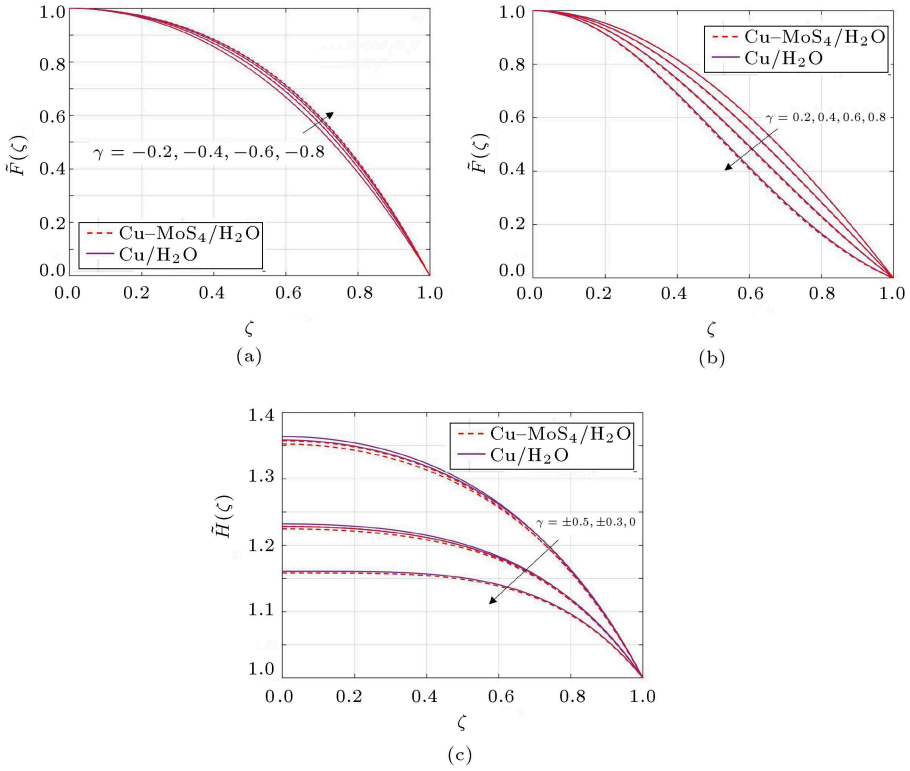

Figure 3. $\tilde{F}'(\zeta)$ and $\tilde{H}(\zeta)$ as a function of γ.

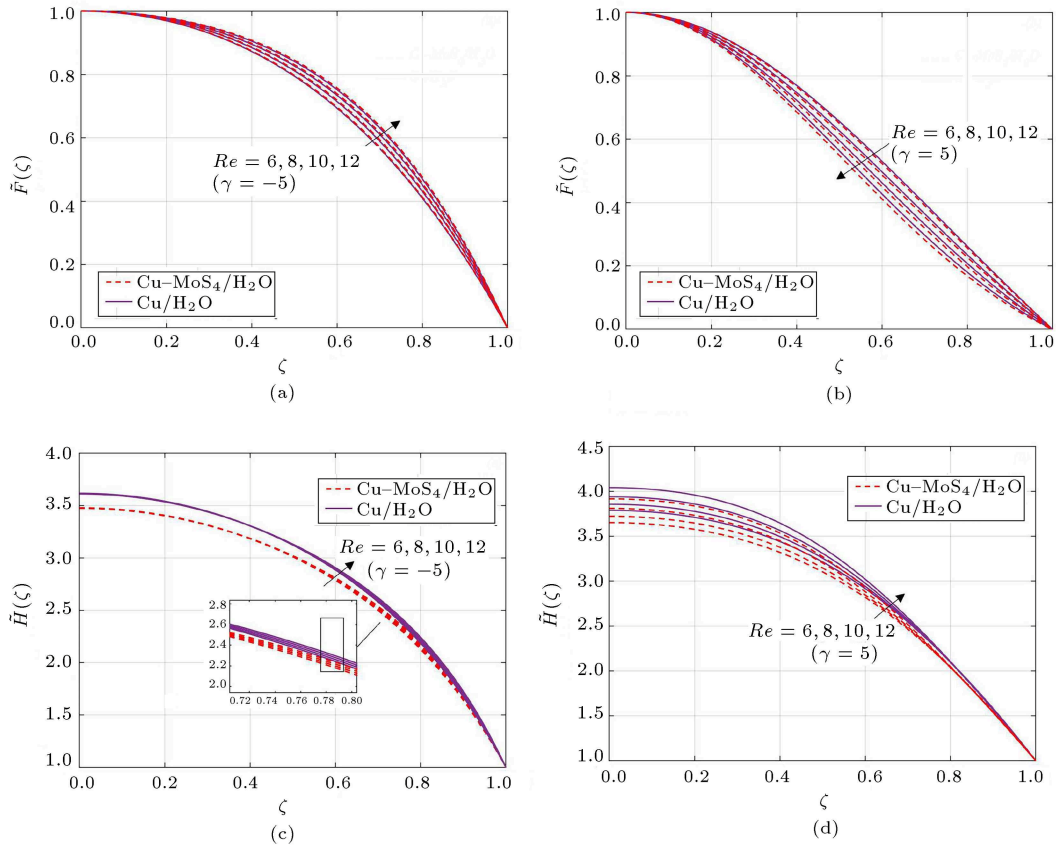

Figure 4. $\tilde{F}'(\zeta)$ and $\tilde{H}(\zeta)$ as a function of Re for $\gamma < 0$ and $\gamma > 0$.

as the fluid moves away from the wall. This behavior is seen for both CC and DC. Similarly, thermal transport is reduced because the values of γ increase as the heat transfer through convection declines as shown in Figure 3(c).

Figure 4(a)–(d) show the relationship of Reynolds number Re on $\tilde{F}'(\zeta)$ and $\tilde{H}(\zeta)$ respectively. Figure 4(a) and (b) show how the presence of Re affects the velocity profile. It is seen that with a high Reynolds number, the velocity profile rises in the case of the CC. However, for $\gamma > 0$, the opposite behavior is noticed. Increasing the values of Re elevates the temperature field in the DC. Furthermore, the motion of the flows is in the other direction, and low temperature is recorded for higher values of Re. A better temperature distribution is shown for the DC as a result of increased Re. On the contrary, an increase in Re in the CC is noticed due to a drop in temperature. This means that the higher the fluid's velocity, the hotter it gets. In a CC, temperature against Re behaves in an entirely different way than in a DC. Moreover, mass transport decreased for $\gamma < 0$ whereas it increased for $\gamma > 0$.

Figure 5(a) and (b) show the impact of Brinkman number Br on thermal energy transport. The Brinkman number is widely utilized in polymer processing and demonstrates the heat conduction from a wall to a fluid motion. It is the ratio between heat generated via viscous dissipation and heat transferred by conduction. In simple words, it is the ratio of heat production to external heating. The higher the value of Br, the slower the heat produced by viscous dissipation is transferred, and hence the temperature rises significantly. The temperature distribution for $\gamma > 0$ is more progressive than $\gamma < 0$. Furthermore, thermal transport for (Cu–MoS$_4$/H$_2$O) is greater than (Cu/H$_2$O). Figure 5(c)–(f) show how the Brinkman number has affected the thermodynamic irreversibility factors for $\gamma > 0$ and $\gamma < 0$. The entropy generation is seen to be a rising function of Br, while the Bejan number has a decreasing trend. As a result of this, the system produces more heat, which increases entropy. Physically, the Brinkman number is connected to heat conduction from a wall to a flowing viscous fluid.

The phenomena of heat transmission have improved as a result of an increase in R_d shown in Figure 6(a) and (b). The conduction of heat transfer to thermal radiation transport is characterized by the radiation parameter. A rising temperature profile results from increasing radiation parameters for $\gamma > 0$ and $\gamma < 0$. Figure 6(c)–(f) depict the variations in $\tilde{E}_n(\zeta)$ and $\tilde{B}_e(\zeta)$ as the radiation parameter rises. $\tilde{B}_e(\zeta)$ exhibits a decreasing tendency via rising R_d; however, entropy generation $\tilde{E}_n(\zeta)$ exhibits the opposite trend. Thermal irreversibility rises as a result of the system

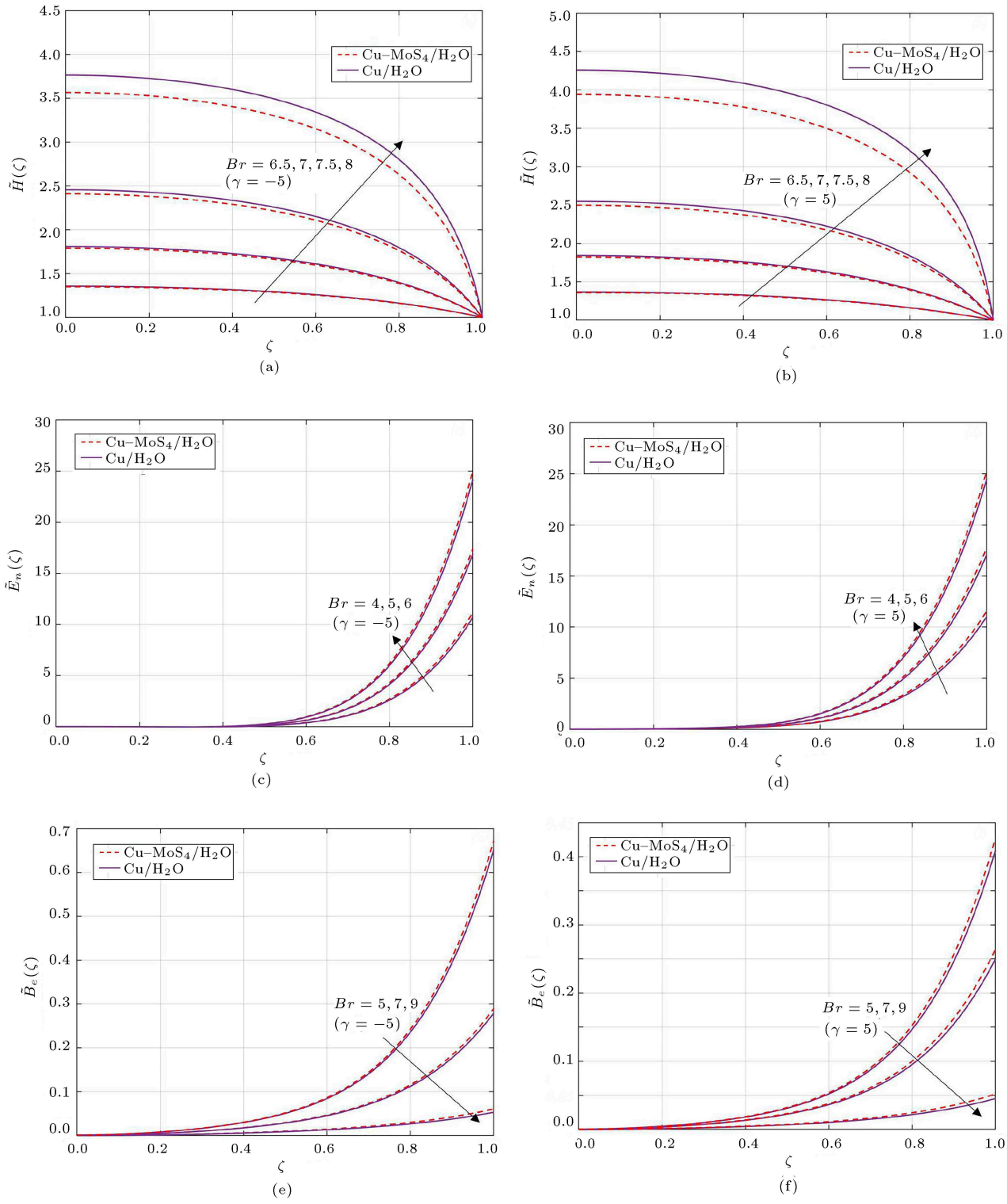

Figure 5. $\tilde{H}(\zeta)$, $\tilde{E}_n(\zeta)$, and $\tilde{B}_e(\zeta)$ as a function of Br for $\gamma < 0$ and $\gamma > 0$.

being heated up more by the radiation parameter for $\gamma > 0$ and $\gamma < 0$. Copper and molybdenum can survive radiation-induced swelling better. Compounds based on copper and molybdenum may have a lot of promise for usage as structural materials to improve reactor systems.

Through the physical sense, the angle of inclination γ has a significant impact on skin friction. The comparison table is constructed from Refs. [23,24] in Table 2. The results obtained are similar to those found in the literature. It is seen that for $\gamma > 0$ the values of $\tilde{F}''(0)$ enhanced due to an increment in Re.

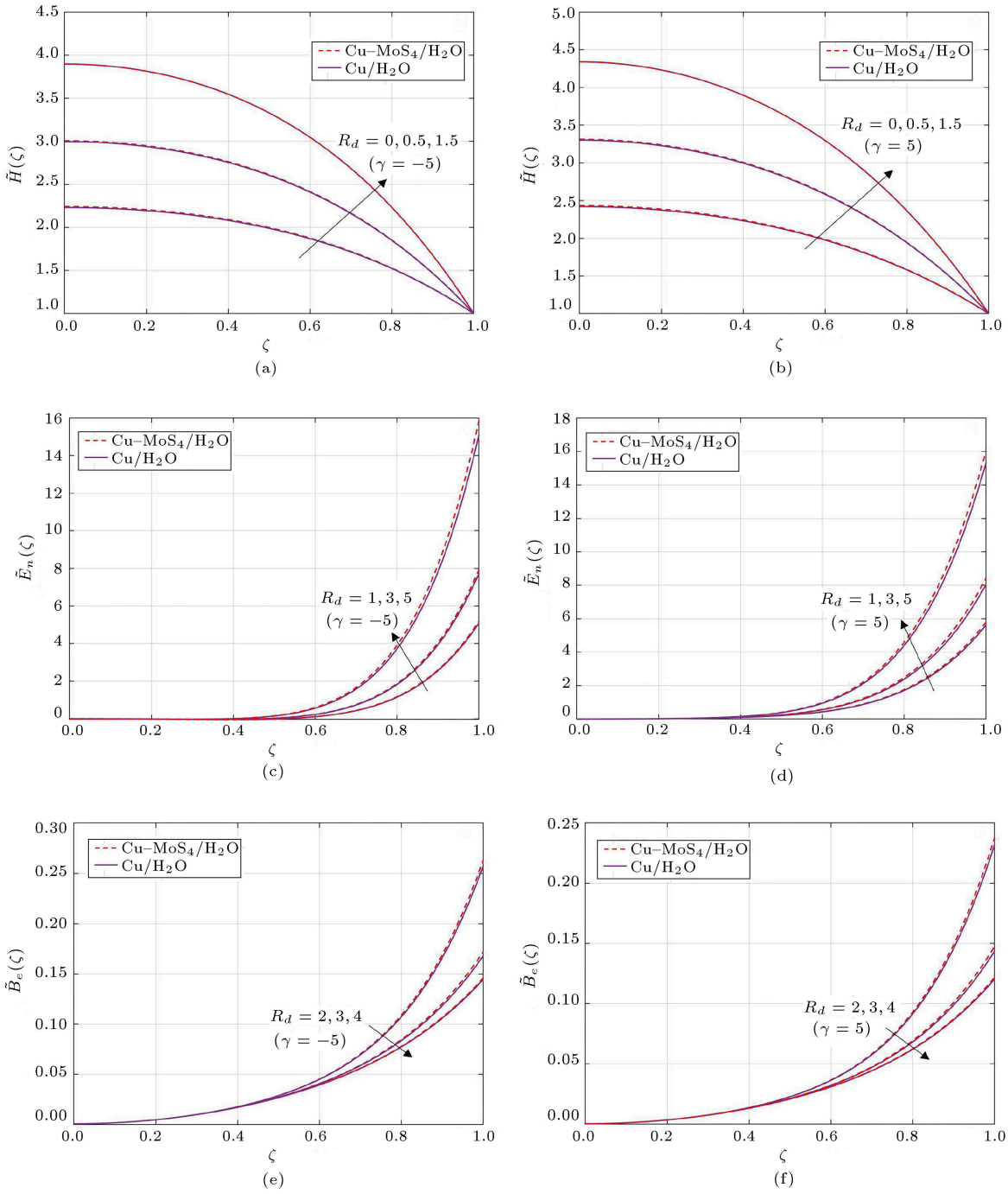

Figure 6. $\tilde{H}(\zeta)$, $\tilde{E}_n(\zeta)$, and $\tilde{B}_e(\zeta)$ as a function of R_d for $\gamma < 0$ and $\gamma > 0$.

However, the opposite behavior is noticed for $\gamma < 0$. The outcomes of small-Re are also given in Table 3. It is seen that the asymptotic behavior reaches its numerical outcome at small-Re. Table 3 contains the behavior of $-\tilde{H}^{'}(1)$ for Br, Re, and R_d. The thermal transport rate is boosted by raising Br and R_d while for both cases, they are declined as Re is increased at $\phi_{Cu} = \phi_{MoS_4} = 0.01$. The outcomes of small-$Re$ are computed, which are in great agreement with their numerical outcomes.

4. Concluding remarks

This study intended to discuss the flow and thermal transport of water-based nanofluids on a wedged-shaped channel. Engine oil was utilized as base fluid, and two types of nanoparticles, Cu and MoS_4, were added. Nanofluid analysis was carried out by incorporating the dissipation effects. The thermophysical characteristics were noted by using the Yamada-Ota model. The exact solution was computed for velocity

Table 2. Comparison of $\tilde{F}''(0)$ with Refs. [23,24] at $\phi_{Cu} = \phi_{\mathbf{MoS_4}} = 0.0$..

$\tilde{F}''(0)$ at $\gamma = 5.0$					$\tilde{F}''(0)$ at $-\gamma = 5.0$				
Re	**Ref. [23]**	**Ref. [24]**	**Present**	**Small-*Re***	***Re***	**Ref. [23]**	**Ref. [24]**	**Present**	**Small-*Re***
20	2.527192	2.527192	2.527189	2.578907	10	1.784547	1.784547	1.784540	1.789769
60	3.942140	3.942140	3.942142	3.959898	30	1.413692	1.413692	1.413693	1.47975
100	5.869165	5.869165	5.869170	5.876377	50	1.121989	1.121989	1.121985	1.127456
140	8.207326	8.207326	8.207324	–	70	0.893474	0.893474	0.893470	–
180	10.792073	10.792073	10.79207	–	100	0.640178	0.640178	0.640179	–

Table 3. Behavior of $\tilde{H}'(1)$ at $\phi_{Cu} = \phi_{\mathbf{MoS_4}} = 0.01, R_d = 0$..

$\tilde{H}'(1)$						
			Numerical values		**Small-*Re* asymptotes**	
Re	***Br***	***R_d***	**(Cu/H_2O)**	**(Cu–MoS_4/H_2O)**	**(Cu/H_2O)**	**(Cu–MoS_4/H_2O)**
1.0	4.0	0.0	−6.465551	−6.559974	−6.44232	−6.562292
2.0			−6.333459	−6.427350	−6.333128	−6.451067
5.0			−5.987070	−6.078801	−5.917185	−6.006165
10.0			−5.630114	−5.715428	−5.617249	−5.783715
1.0	4.0	0.0	−6.465551	−6.559974	−6.44232	−6.562292
	5.0		−8.081938	−8.199968	−8.063833	−8.163936
	6.0		−9.698326	−9.839961	−9.6766	−9.899051
1.0	4.0	0.0	-6.465551	−6.559974	−6.44232	−6.562292
		0.5	−5.107501	−5.129965	−5.161264	−5.183715
		1.5	−3.149547	−3.175335	−5.183715	−3.270023

equations, and the numerical solution was developed by applying the bvp4c built-in MATLAB. The numerical outcomes of WSP and Nusselt number were determined as functions of pertinent parameters. The following are the primary conclusions:

- The flow and temperature fields were reduced due to the addition in the nanoparticles volume fraction for both (Cu–MoS_4/H_2O) and (Cu/H_2O) cases;
- Heat transport was diminished by incrementing the angle of inclination. However, enhancing the Reynolds number caused the elevation of the temperature distribution;
- Thermal transport and entropy generation were an increasing function of Brinkman number and radiation parameter for both profiles of nanofluids and channels;
- Bejan number decremented due to Brinkman number and radiation parameter for convergent-divergent channels;
- The temperature gradient was developed for both convergent and divergent channels;
- The hybrid nanofluid (Cu–MoS_4/H_2O) profile was dominated over the simple-mono (Cu/H_2O) nanofluid profile;
- For the divergent channel, the numerical outcomes of the coefficient of skin friction were enhanced due to the Reynolds number, but for the convergent channel, it was reduced;
- By incrementing the Brinkman number and radiation parameter, the numerical outcomes of the heat transfer rate were improved; however, the opposite behavior was depicted for the Reynolds number;
- The asymptotic values of the coefficient of skin friction and heat transfer rates approached their numerical behavior for small values of Reynolds number.

Nomenclature

(r, ϑ, z)	Cylindrical polar coordinates
V	Velocity field (ms^{-1})
$\tilde{T}_{wall}$	Upper wall temperature (K)
μ	Dynamic viscosity ($kgm^{-1}s^{-1}$)
ϱ	Fluid density (kgm^{-3})
c_p	Specific heat capacity ($Jkg^{-1}K^{-1}$)
$\tilde{f}_{\max}$	Dimensional constant
Br	Brinkman number

Re	Reynolds number
$-\tilde{H}^{'}(1)$	Heat transfer rate
$C_{\tilde{f}}$	Coefficient of skin friction
$\tilde{F}^{'}(\zeta), \tilde{H}(\zeta)$	Dimensionless velocity and temperature
ζ	Dimensionless variable
$\tilde{T}$	Fluid temperature (K)
$\tilde{U}_{\max}$	Velocity at centerline (ms^{-1})
k	Thermal conductivity ($Wm^{-1}K^{-1}$)
p	Fluid pressure (Nm^{-2})
γ	Angle of inclination (deg or rad)
ψ_q	Heat flux
Ec	Eckert number
Pr	Prandtl number
Nu	Nusselt number
τ_{wall}	Wall-shear stress

Subscripts

r	Derivative w.r.t r
w	Condition at wall
n	Nanofluid
ϑ	Derivative w.r.t ϑ
hn	Hybrid nanofluid
f	Fluid

Superscripts

$'$	Derivative with respect to ζ

Abbreviations

J-H	Jeffery-Hamel
CC	Convergent Channel
BCs	Boundary Conditions
WSP	Wall Stress Parameter
CNT	Carbon nanotubes
MHD	Magnetohydrodynamic
DC	Divergent Channel
PDEs	Partial Differential Equations
ODEs	Ordinary Differential Equations

References

1. Jeffery, G.B.L. "The two-dimensional steady motion of a viscous fluid", *Lond. Edinb. Dublin Philos. Mag. J. Sci.*, **29**(172), pp. 455–465 (1915).
2. Hamel, G., Spiralformige, B., and Zaher, F. "Ders-deutschen jahresbericht", *Math. Ver.*, **25**, pp. 34–60 (1916).
3. Axford, W. "The magnetohydrodynamic Jeffrey-Hamel problem for a weakly conducting fluid", *Q. J. Mech. Appl. Math.*, **14**(3), pp. 335–351 (1961)
4. Hamadiche, M., Scott, J., and Jeandel, D. "Temporal stability of Jeffery-Hamel flow", *Journal of Fluid Mechanics*, **268**, pp. 71–88 (1994).
5. Makinde, O.D. and Mhone, P.Y. "Hermite-Padé approximation approach to MHD Jeffery-Hamel flows", *Appl. Math. Comput.*, **181**(2), pp. 966–972 (2006).
6. Esmaeilpour, M. and Ganji, D.D. "Solution of the Jeffery-Hamel flow problem by optimal homotopy asymptotic method", *Comput. Math. with Appl.*, **59**(11), pp. 3405–3411 (2010).
7. Mahmood, A., Md Basir, M.F., Ali, U., et al. "Numerical solutions of heat transfer for magnetohydrodynamic Jeffery-Hamel flow using spectral homotopy analysis method", *Processes*, **7**(9), p. 626 (2019).
8. Ellahi, R. "Exact and numerical solutions for nonlinear differential equation of Jeffrey-Hamel flow", **3**(1), pp. 1–7 (2011).
9. Abbasbandy, S. and Shivanian, E. "Exact analytical solution of the MHD Jeffery-Hamel flow problem", *Meccanica*, **47**(6), pp. 1379–1389 (2012).
10. Bougoffa, L., Mziou, S., and Rach, R.C. "Exact and approximate analytic solutions of the Jeffery-Hamel flow problem by the Duan-Rach modified Adomian decomposition method", *Math. Model. Anal.*, **21**(2), pp. 174–1787 (2016).
11. Amiri Rad, E., Mahpeykar, M.R., and Teymourtash, A.R. "Analytic investigation of the effects of condensation shock on turbulent boundary layer parameters of nucleating flow in a supersonic convergent-divergent nozzle", *Sci. Iran.*, **21**(5), pp. 1709–1718 (2014).
12. Heydari, M.M. "Investigation of fluid flow and heat transfer of compressible flow in a constricted microchannel", *Sci. Iran.*, **23**(5), pp. 2144–2153 (2016).
13. Ahmad, S., Hayat, T., Alsaedi, A., et al. "Finite difference analysis of time-dependent viscous nanofluid flow between parallel plates", *Commun. Theor. Phys.*, **71**(11), p. 1293 (2019).
14. Choi, S.U. and Eastman, J.A. "Enhancing thermal conductivity of fluids with nanoparticles", *Developments and Applications of Non-Newtonian Flows*, **231**(66), pp. 99–105 (1995).
15. Sheikholeslami, M., Ganji, D.D., Ashorynejad, H.R., et al. "Analytical investigation of Jeffery-Hamel flow with high magnetic field and nanoparticle by Adomian decomposition method", *Appl. Math. Mech.*, **33**(1), pp. 25–36 (2012).
16. Kumar, K.G., Rahimi-Gorji, M., Reddy, M.G., et al. "Enhancement of heat transfer in a convergent/divergent channel by using carbon nanotubes in the presence of a Darcy-Forchheimer medium", *Microsyst. Technol.*, **26**(2), pp. 323–332 (2020).
17. Sarfraz, M., Khan, M., and Muhammad, Y. "Dynamics of water conveying iron oxide and graphene nanoparticles subject to stretching/spiraling surface: An asymptotic approach", *Ain Shams Eng. J.*, **14**(8), 102021 (2022).

18. Akinshilo, A.T., Ilegbusi, A., Ali, H.M., et al. "Heat transfer analysis of nanofluid flow with porous medium through Jeffery Hamel diverging/converging channel", *J. Appl. Comput. Mech.*, **6**(3), pp. 433–444 (2022).

19. Khan, M., Sarfraz, M., Ahmed, A., et al. "Study of engine-oil based CNT nanofluid flow on a rotating cylinder with viscous dissipation", *Phys. Scr.*, **96**(7), 075005 (2021).

20. Berrehal, H. and Makinde, O.D. "Heat transfer analysis of CNTs-water nanofluid flow between nonparallel plates: Approximate solutions", *Heat Transf.*, **50**(5), pp. 4978–4992 (2021).

21. Das, A.C. and Nasa, Q.N. "Analysis of magnetohydrodynamic Jeffery-Hamel flow in a convergent-divergent channel using Cu-water nanofluid", *J. Eng. Sci.*, **12**(2), pp. 79–92 (2021).

22. Shampine, L.F., Kierzenka, J., and Reichelt, M.W. "Solving boundary value problems for ordinary differential equations in MATLAB with bvp4c", Tutorial notes 2000, pp. 1–27 (2000).

23. Motsa, S.S., Sibanda, P., and Marewo, G.T. "On a new analytical method for flow between two inclined walls", *Numer. Algorithms*, **61**(3), pp. 499–514 (2012).

24. Khan, U., Ahmed, N., and Mohyud-Din, S.T. "Heat transfer effects on carbon nanotubes suspended nanofluid flow in a channel with non-parallel walls under the effect of velocity slip boundary condition: a numerical study", *Neural Comput. Appl.*, **28**(1), pp. 37–46 (2017).

Biographies

Mahnoor Sarfraz is PhD scholar at the Department of Mathematics, Quaid-i-Azam University, Islamabad 44000, Pakistan. She is pursuing a doctorate in Applied Mathematics , majorly Fluid Mechanics. Her research deals with applications of Physics and Mathematics in Engineering.

Masood Khan is a Professor at the Department of Mathematics, Quaid-i-Azam University, Islamabad 44000, Pakistan. His research interests are Non-Newtonian Fluid Mechanics, Bio-Mechanics, Blood Flow Problems, Computational Fluid Dynamics, Homotopy Analysis Method, Homotopy Perturbation Method, Mathematical Modeling, Peristaltic Motion, and Symmetry Methods for Differential Equations.